Detecting the stiffness and mass of biochemical adsorbates by a resonator sensor

Yin Zhang*

State Key Laboratory of Nonlinear Mechanics (LNM), Institute of Mechanics, Chinese Academy of Sciences, Beijing 100190, China

ABSTRACT

The biochemical adsorption on a resonator sensor can result in the changes of both stiffness and mass. If the effect of stiffness is not considered, the resonator response will be wrongly interpreted. Determining the adsorbate stiffness and mass by the shifts of resonant frequency formulates an inverse problem. The inverse problem is solved by varying the adsorbate thickness and measuring the corresponding shifts of resonant frequencies. With the technique of solving the inverse problem, a micro/nanomechanical resonator can be used to identify what kind of material an adsorbate is, which is more than a mass resonator sensor.

© 2014 Elsevier B.V. All rights reserved.

1. Introduction

Micro/nanomechanical resonator provides a label-free, high throughput and rapid detection of biological and chemical molecules [1,2]. When a resonator structure is scaled down in size, the resonant frequency increases, which also leads to a higher sensitivity [3]. The micro/nanomechanical resonators with the capability of detecting the presence of a biomolecule [2], a cell [4], a virus [5], a protein [6] and a gold atom [7], have been developed. A recent record of sensitivity was achieved by a carbon nanotube (CNT) based nanomechanical resonator, which can detect the mass of a single proton [8]. The sensing mechanism of all above micro/nanomechanical resonators [1–8] is based on the following equation

$$\frac{\Delta\omega}{\omega_o} \approx -\frac{1}{2}\frac{\Delta m}{m},\tag{1}$$

where ω_o is the circular resonant frequency without adsorption and $\Delta\omega$ is the resonant frequency shift due to adsorption; m is the (known) effective sensor mass and Δm is the (unknown) effective adsorbed mass. Once ω_o and $\Delta\omega$ are measured, Δm is uniquely determined by the above equation. The implicit assumption of Eq. (1) is that adsorption only induces the mass addition; the resonator based on Eq. (1) is a mass resonator sensor. However,

the mass information only is insufficient to provide fundamental insights into the resonator-based molecular detection [9]. In general, the appropriate properties of a detected material including its mechanical properties as well as the mass must be considered when interpreting the resonator data [10]. A vivid example is that in their pioneering experiment, Ramos et al. [11] found that the adsorption of the *Escherichia coli* (*E. coli*) bacteria on a silicon resonator causes the increase of resonant frequency. According to Eq. (1), the mass addition due to adsorption can only decrease the resonant frequency. The increase of resonant frequency can only mean that the stiffness of the bacteria plays a more important or even a dominant role [11,12]. Similarly, the adsorption of organic molecules (alkanethiol) also causes the increase of resonant frequency [12]. Even for the resonant frequency decreasing cases, if the stiffness effect is not considered, the mass can be significantly underestimated [12,13]. Furthermore, in the adsorption tests of various proteins, it has also been found that the mass addition alone cannot explain the (anomalous) shifts of the resonant frequencies [14,15].

When adsorption occurs, the stiffness, mass and damping of the system change and the resonant frequency is given as follows [16]

$$\omega' = \sqrt{\frac{k+\Delta k}{m+\Delta m}}\sqrt{1-\frac{(C+\Delta C)^2}{4mk}},\tag{2}$$

ω' is the circular resonant frequency after adsorption ($\Delta\omega = \omega' - \omega_o$). k, m and C are the effective spring stiffness, mass and damping of a resonator, respectively. Δk, Δm and ΔC are those corresponding changes due to adsorption. The mechanisms for the damping variation are rather complex and still unclear

* Tel.: +86 10 82543970.
  E-mail address: zhangyin@lnm.imech.ac.cn

for micro/nanomechanical resonator [16,17]. When a resonator motion is measured in an experiment, C and ΔC can be extracted by the half-power method [18]. The reason for the mass change in an adsorption process is obvious. The stiffness change is mainly caused by two mechanisms: the adsorbate stiffness [11,12] and surface stress [19,20]. The adsorbate stiffness always increases the resonant frequency. Because surface stress can be either tensile or compressive [21,22], it can either increase or decrease the stiffness [19,23,24]. It is worth mentioning here that the heated debates on whether surface stress can be modelled as an axial load on a cantilever beam, which can thus change the stiffness, are still being exchanged [23,25,26]. However, in a clamped-clamped beam, there is no doubt that surface stress can result in the stiffness change [25,26]. There are other scenarios which can also cause the stiffness change. For example, because a coating polymer layer absorbs vapor molecules, which results in swelling and thus compressive force, the resonator stiffness decreases significantly [27]. In the forward problem in which Δk, Δm and ΔC are given, ω' is uniquely determined by Eq. (2). However, in the real application of a resonator, ω', k, m, C and ΔC are the (known) measured quantities; Δk and Δm are the two unknown quantities to be determined. For a given/measured ω', there are infinite combinations of Δk and Δm. Therefore, in order to characterize more properties of adsorbate, we encounter the following inverse problem in practice: *How to use the shifts of resonant frequencies to determine the stiffness and mass of adsorbate?* A similar inverse problem was also raised by Chen et al. [28]. Because of the formation of amalgamation in the mercury adsorption test [28,29] and the formation of hydride in the hydrogen adsorption test, the stiffness and mass of a micromechanical sensor often change together in those vapor adsorption tests and the inverse problem thus arises naturally. In contrast, in the mass resonator case, there is no such inverse problem because Δm is the only unknown variable, which is uniquely determined by the resonant frequency shift.

In Ramos' experiment [11], they counted the total *E. coli* bacteria number (about 4200) and calculated the mass; the bacteria stiffness was then obtained by curve-fitting, which in essence is still a forward problem. They changed the adsorption location to try to "uncouple" the effects of stiffness and mass of the bacteria [11]. As shown later in this study, the methods including shifting adsorption location, multiple resonant frequencies and changing

the adsorption length can not be used to solve the inverse problem. By varying the adsorbate thickness and utilizing a geometric approximation, a solution method to the inverse problem is presented and its accuracy is also demonstrated. The advantages of solving the inverse can be the following two: (1) the application of a micro/nanomechanical resonator can be extended beyond mass sensing. (2) Because the stiffness and mass of adsorbate are among the most difficult quantities to be measured in the resonator application, our method, which only requires the measurement of the resonant frequency and adsorbate thickness, is expected to reduce extra experimental instruments and relieve some laborious efforts.

2. Model development

Fig. 1(a) is a schematic of a cantilever beam with an adsorbate layer ranging from x_s to x_e. The governing equation is thus divided into three domains as follows [11,12]

$$
\begin{cases}
m\dfrac{\partial^2 w_1}{\partial t^2} + D\dfrac{\partial^4 w_1}{\partial x^4} = 0, & 0 \le x \le x_s \\[2mm]
(m+\Delta m)\dfrac{\partial^2 w_2}{\partial t^2} + (D+\Delta D)\dfrac{\partial^4 w_2}{\partial x^4} = 0, & x_s \le x \le x_e \\[2mm]
m\dfrac{\partial^2 w_3}{\partial t^2} + D\dfrac{\partial^4 w_3}{\partial x^4} = 0, & x_e \le x \le L
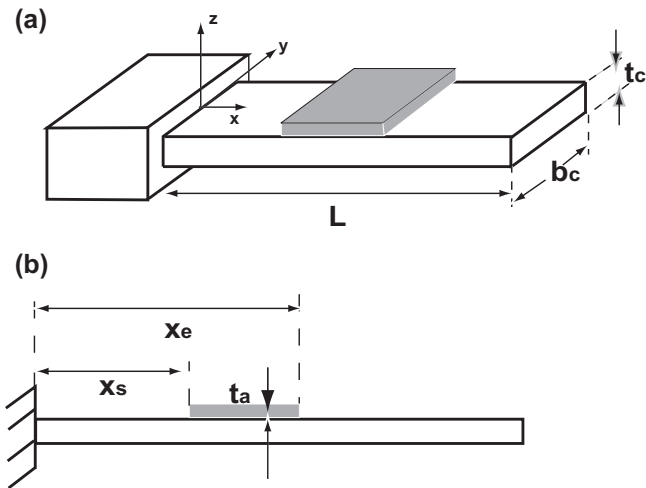\end{cases}
\tag{3}
$$

where w_i (i = 1, 2, 3) is the beam deflection in different domains and L is the beam length; m is the beam mass per unit length and $m = \rho_c b_c t_c$ (ρ_c, b_c and t_c are the mass density, width and thickness of the beam, respectively). Δm is the mass per unit length of the adsorbate layer and $\Delta m = \rho_a b_a t_a$ (ρ_a, b_a and t_a are the mass density, width and thickness of the adsorbate layer, respectively). $D = E_c b_c t_c^3 / 12$ is the beam bending stiffness and E_c is the beam Young's modulus. ΔD is the stiffness change due to the adsorbate layer, which is given as the following [11,12]

$$
\Delta D = \frac{b_c}{12}\frac{E_c^2 t_c^4 + E_a^2 t_a^4 + 2E_c E_a(2t_c^2 + 3t_c t_a + 2t_a^2)}{E_c t_c + E_a t_a} - D.
\tag{4}
$$

Here E_a is the Young's modulus of the adsorbate layer, which is assumed to have the same width as that of the beam. Here the stiffness change due to surface stress is not considered. Because the surface of the silicon resonator is not functionalized, the surface stress induced by the adsorbate materials as discussed in this study is very small [11,12]. Surface stress is the sensing mechanism for many receptor-based sensors [21,22]. However, the receptor–ligand binding is highly selective for identifying an adsorbate/ligand; the challenges for developing robust and stable recognition methods through functionalized coatings (i.e., the receptor materials) and even interpreting the responses of receptor-based sensor still remain [30]. The development for the receptor-less or receptor-free sensors, which bypass the chemistry of receptor–ligand binding and capitalize on the intrinsic material properties of adsorbate, has been called for [30]. Here the mass density (related with mass) and Young's modulus (related with stiffness) are the intrinsic material properties, which can be used to identify the material of an adsorbate.

By introducing $\xi = x/L$, $\tau = \sqrt{EI/(mL^4)}t$ and $W = w/L$ [23,24], Eq. (3) is nondimensionalized as follows

$$
\begin{cases}
\dfrac{\partial^2 W_1}{\partial \tau^2} + \dfrac{\partial^4 W_1}{\partial \xi^4} = 0, & 0 \le \xi \le \xi_s \\[2mm]
(1+\beta)\dfrac{\partial^2 W_2}{\partial \tau^2} + (1+\alpha)\dfrac{\partial^4 W_2}{\partial \xi^4} = 0, & \xi_s \le \xi \le \xi_e \\[2mm]
\dfrac{\partial^2 W_3}{\partial \tau^2} + \dfrac{\partial^4 W_3}{\partial \xi^4} = 0, & \xi_e \le \xi \le 1
\end{cases}
\tag{5}
$$

Fig. 1. (a) Schematic diagram of a cantilever resonator with molecules adsorbed on its surface and the coordinate system. E_c, E_a and ρ_c, ρ_a are the Young's moduli and densities of the resonator and adsorbed layer, respectively. l_c, b_c and t_c are the resonator length, width and thickness, respectively. (b) The adsorbed layer is (assumed) uniformly distributed from x_s to x_e with a thickness of t_a and a width of $b_a = b_c$.

where $\xi_s = x_s/L$ and $\xi_e = x_e/L$; α and β are the dimensionless quantities defined as follows

$$\alpha = \frac{\Delta D}{D}$$
$$= \frac{(E_a/E_c)^2(t_a/t_c)^4 + (E_a/E_c)(t_a/t_c)[3 + 6(t_a/t_c) + 4(t_a/t_c)^2]}{1 + (E_a/E_c)(t_a/t_c)},$$

$$\beta = \frac{\Delta m}{m} = \frac{\rho_a t_a}{\rho_c t_c}. \tag{6}$$

Physically, α and β are the stiffness and mass ratios of the adsorbate layer to the beam, respectively. Here α and β are constants, which is based on the following two assumptions: (1) the adsorbate layer is uniformly distributed along $\xi_s \leq \xi \leq \xi_e$. (2) The inkjetted biological and chemical samples are in a stable equilibrium state. It can take minutes or even hours for the samples to reach an equilibrium state [31]. During the transient state, the adsorbate layer experiences the conformation changes, which often leads to the variations of surface stress and the layer stiffness because different layer structures are formed [20,31].

Due to the presence of the adsorbate layer, the mode shapes of the system vary as a function of the layer dimensions and locations. In the numerical methods such as Rayleigh–Ritz method [11,12] and Galerkin method [23,24], the accuracy of the computed eigenfrequencies depends on the accuracy of the mode shape [23]. A tiny deviation from the exact mode shape causes a tiny relative error in the eigenfrequency computation. However, even a tiny computation error is unacceptable in the micro/nano mass resonator application. One of great advantages of the micro/nano mass resonator sensor is to detect the tiny fractional change. For the micro/nanoresonator with the eigenfrequency of giga-Hertz (10^9 Hz) or higher [32], the tiny relative error means the mega-Hertz or kilo-Hertz difference, which is absolutely large enough. Furthermore, as shown later, because the organic and biological materials usually have very small Young's modulus, the (relative) resonant frequency shifts are very small. A tiny computation error may lead us to a wrong interpretation of data. Here we present the exact solution to the eigenfrequency, which eliminates the error due to the deviation of mode shape.

By assuming $W = U(\xi)e^{i\omega\tau}$ (ω is the dimensionless circular frequency) and substituting it into Eq. (5), $U(\xi)$ is solved as follows

$$U(\xi) = \begin{cases} U_1(\xi) = A_1 \sin(\kappa_1\xi) + B_1 \cos(\kappa_1\xi) + C_1 \sinh(\kappa_1\xi) + D_1 \cosh(\kappa_1\xi), & 0 \leq \xi \leq \xi_s \\ U_2(\xi) = A_2 \sin(\kappa_2\xi) + B_2 \cos(\kappa_2\xi) + C_2 \sinh(\kappa_2\xi) + D_2 \cosh(\kappa_2\xi), & \xi_s \leq \xi \leq \xi_e \\ U_3(\xi) = A_3 \sin(\kappa_1\xi) + B_3 \cos(\kappa_1\xi) + C_3 \sinh(\kappa_1\xi) + D_3 \cosh(\kappa_1\xi), & \xi_e \leq \xi \leq 1 \end{cases} \tag{7}$$

where $\kappa_1 = \sqrt{\omega}, \kappa_2 = \sqrt[4]{(1+\beta)/(1+\alpha)} \times \sqrt{\omega}$; A_i, B_i, C_i and D_i ($i = 1$, 2 and 3) are the twelve unknown constants in total. To formulate an eigenvalue problem, twelve equations are needed. The boundary conditions of a cantilever give the following four:

$$U_1(0) = 0, \quad \frac{dU_1}{d\xi}(0) = 0, \quad \frac{d^2U_1}{d\xi^2}(1) = 0, \quad \frac{d^3U_1}{d\xi^3}(1) = 0 \tag{8}$$

The matching conditions at ξ_s and ξ_e give the following eight equations [33]:

$$U_1(\xi_s) = U_2(\xi_s), \quad \frac{dU_1}{d\xi}(\xi_s) = \frac{dU_2}{d\xi}(\xi_s), \quad \frac{d^2U_1}{d\xi^2}(\xi_s) = \frac{d^2U_2}{d\xi^2}(\xi_s),$$

$$\frac{d^3U_1}{d\xi^3}(\xi_s) = \frac{d^3U_2}{d\xi^3}(\xi_s) \tag{9}$$

and

$$U_2(\xi_e) = U_3(\xi_e), \quad \frac{dU_2}{d\xi}(\xi_e) = \frac{dU_3}{d\xi}(\xi_e), \quad \frac{d^2U_2}{d\xi^2}(\xi_e) = \frac{d^2U_3}{d\xi^2}(\xi_e),$$

$$\frac{d^3U_2}{d\xi^3}(\xi_e) = \frac{d^3U_3}{d\xi^3}(\xi_e) \tag{10}$$

The eight matching conditions at ξ_s and ξ_e are to guarantee the continuity of displacement, slope, moment and shear force [33]. Now by substituting Eq. (7) into the above twelve equations of Eqs. (8)–(10), the following eigenvalue problem is formed

$$KV = 0. \tag{11}$$

where $\mathbf{V}$ is the vector defined as $\mathbf{V}^T = (A_1, B_1, C_1, D_1, A_2, B_2, C_2, D_2, A_3, B_3, C_3, D_3)$ and $\mathbf{K}$ is a 12×12 matrix as given in Appendix A. When α, β, ξ_s and ξ_e are given, the eigenfrequency ω is computed by Eq. (11), which is a transcendental equation. The Newton–Rhapson method [34] is used here.

3. Results and discussion

In all the figures and results discussed here, the beam is made of silicon with $E_c = 169$ GPa and $\rho_c = 2330$ kg m^{-3} [12]; its dimensions are fixed as $L \times b_c \times t_c = 100$ μm $\times 20$ μm $\times 1$ μm [12]. When $\alpha = \beta = 0$, which is the no adsorbate case, the cantilever first two (dimensionless) resonant frequencies are given as follows [35]:

$$\omega_1^0 = 1.875104^2 = 3.5160153, \quad \omega_2^0 = 4.6940911^2 = 22.0344916. \tag{12}$$

When $\xi_s = 0$ and $\xi_e = 1$, which is the case that the beam is fully covered with an adsorbate layer, it is not hard for us to derive the following equation:

$$\omega_i = \sqrt{\frac{1+\alpha}{1+\beta}}\omega_i^0 \tag{13}$$

where ω_i is the ith resonant frequency with the presence of an adsorbate layer and ω_i^0 is the ith resonant frequency with no adsorbate layer. It is worth pointing out that Eq. (13) applies to all resonant frequencies, which is somewhat surprising. As discussed later, this fact has the implication that the method of multiple resonant frequencies [23,24] cannot be used here to solve the inverse problem. The relative frequency shift is defined as $(\omega_i - \omega_i^0)/\omega_i^0$ and $(\omega_i - \omega_i^0)/\omega_i^0$ versus t_a/t_c is plotted in Fig. 2. Because α and β defined in Eq. (6) vary with t_a/t_c, the resonant frequencies changes. Two adsorbate materials are used: one is the organic layer of alkanethiol with $E_a = 12.9$ GPa and $\rho_a = 675$ kg m^{-3} [12] and the other is the biological layer of myosin with $E_a = 0.7$ GPa and $\rho_a = 183$ kg m^{-3} [12]. The solid line in Fig. 2 is obtained for the myosin layer by setting $\alpha = 0$, which is to show its mass effect only. Clearly, when the stiffness effect is ignored, the actual adsorbate mass can be significantly underestimated for a given frequency shift. The same plot as Fig. 2 was also presented by Tamayo et al. [12]. Our results have (almost) no difference from theirs, which verifies Eq. (13). Furthermore, when $\alpha_1 \ll 1$ and $\beta_1 \ll 1$, Eq. (13) can be approximated as a linear one [19]

$$\sqrt{\frac{1+\alpha}{1+\beta}} - 1 \approx \frac{\alpha}{2} - \frac{\beta}{2} = \frac{\omega_i - \omega_i^0}{\omega_i^0}. \tag{14}$$
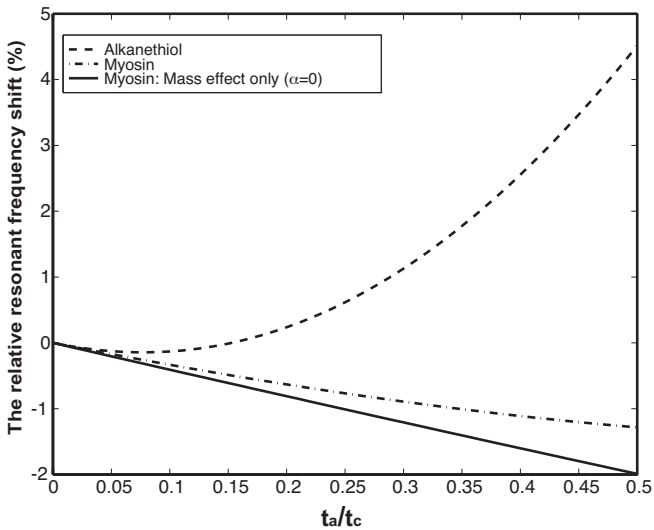
Fig. 2. Relative resonant frequency shifts (%) versus t_a/t_c.

The more general scenario is that the beam is partially covered by an adsorbate layer [11,12]. In Fig. 3, the myosin layer ranges from $\xi_s = 0.7$ to $\xi_e = 0.9$ with $t_a/t_c = 0.1$. Therefore, $\alpha = 1.5070698 \times 10^{-3}$ and $\beta = 8.206278 \times 10^{-3}$ are calculated by Eq. (6). By substituting the values of ξ_s, ξ_e, α and β into Eq. (11), the first and second resonant frequencies are computed as $\omega_1 = 3.5110114$ and $\omega_2 = 22.0305723$. Both resonant frequencies decrease after the beam is covered with the myosin layer. Compared with ω_1^0 and ω_2^0 as given in Eq. (12), the relative shifts of ω_1 and ω_2 are −0.142% and −0.018%, respectively. Unlike the full coverage scenario that all resonant frequencies have the same the relative shift of $\sqrt{(1+\alpha)/(1+\beta)} - 1$ as indicated by Eq. (13), in the

partial coverage scenario the relative shifts are different for different resonant frequencies. However, $(\alpha, \beta) = (1.5070698 \times 10^{-3}, 8.206278 \times 10^{-3})$ is not the only combination which causes the two resonant frequencies to change to $\omega_1 = 3.5110114$ and $\omega_2 = 22.0305723$. Fig. 3(a) plots the changes of the first resonant frequency (ω_1) as α ranges from 0 to 8×10^{-3} and β ranges from 0 to 0.02. Clearly, ω_1 increases monotonically along the α-axis and decreases monotonically along the β-axis. It is easy to understand because the increase of stiffness/mass always results in the increase/decrease of resonant frequencies. The level plane is the one with the fixed value of $\omega_1 = 3.5110114$. The intersection of the two planes is marked as a solid line, which physically indicates that the combinations of α and β resulting in $\omega_1 = 3.5110114$ are infinite. Similarly, in Fig. 3(b), the level plane is the one with the fixed value of $\omega_2 = 22.0305723$; the intersection of the two planes leads to a line indicating the α-β combinations of resulting in $\omega_2 = 22.0305723$. If the two lines obtained in Fig. 3(a) and (b) are projected into the $\alpha - \beta$ plane, they are the same. We can continue the same procedure for other higher resonant frequencies, which will generate the same intersection line, too. This fact in essence is to say that the method of using the shifts of different resonant frequencies [23,24] to solve the inverse problem does not work here. The method [23,24] works because the responses of different resonant frequencies to surface stress (modeled as an axial load) are different. Now let us explain why the method does not work for the inverse problem here. In practice, ξ_s, ξ_e, ω_i^0 and ω_i are the measured quantities; for a given adsorbate layer, α and β are fixed but unknown. Therefore, according to Eq. (13) for the full coverage scenario, no matter how many ω_is are measured, they all lead to the same one equation of $\sqrt{(1+\alpha)/(1+\beta)} = \omega_i/\omega_i^0$ and mathematically, two unknown variables (α and β) cannot be solved by one equation. Similarly, in the partial coverage scenario, the effects of two parameters of α and β are combined into one parameter of κ_2 as given in Eq. (7).
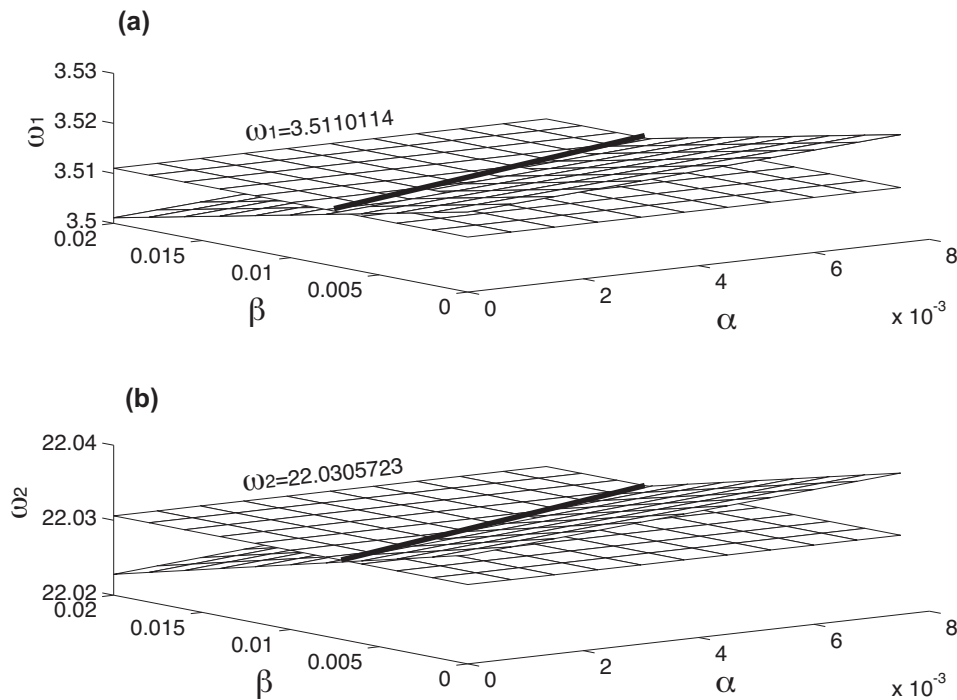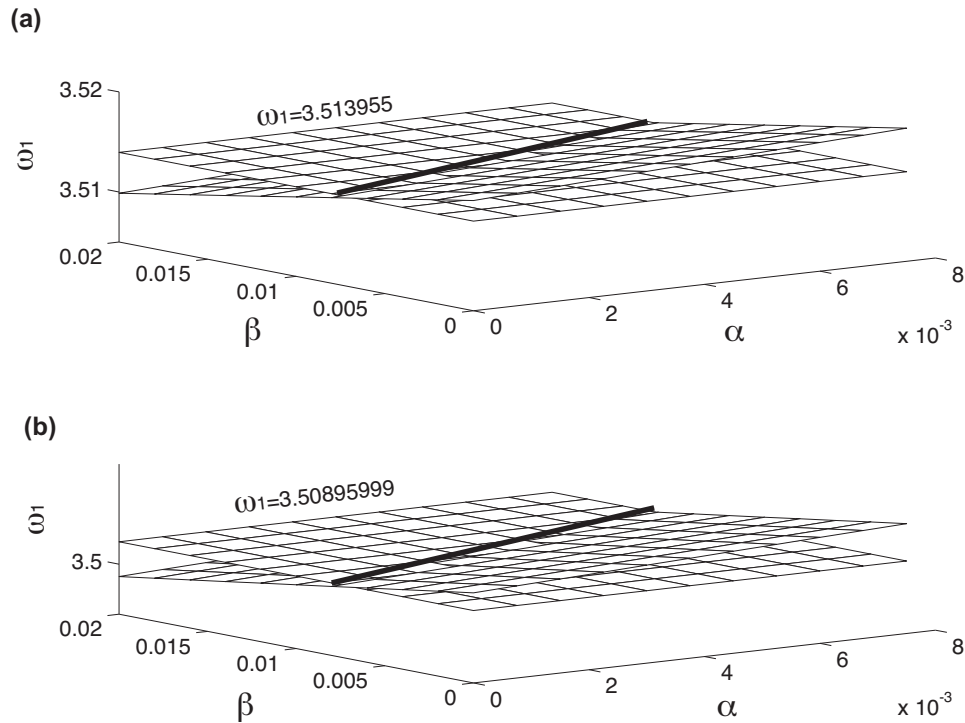
(a)

(b)

Fig. 3. (a) Variation of the first resonant frequency (ω_1) as a function of α and β. The level plane is the one with a fixed resonant frequency of $\omega_1 = 3.5110114$. The intersection of the two planes is marked with a solid line. (b) Variation of the second resonant frequency (ω_2) as a function of α and β. The level plane is the one with a fixed resonant frequency of $\omega_2 = 22.0305723$. For both (a) and (b), $t_a/t_c = 0.1$, $\xi_s = 0.7$ and $\xi_e = 0.9$ are fixed.

(a)

(b)

Fig. 4. (a) Variation of the first resonant frequency (ω_1) as a function of α and β. The level plane is the one with a fixed resonant frequency of $\omega_1 = 3.513955$. $t_a/t_c = 0.1$, $\xi_s = 0.5$ and $\xi_e = 0.7$. The intersection of the two planes is marked with a solid line. (b) Variation of the first resonant frequency (ω_1) as a function of α and β. The level plane is the one with a fixed resonant frequency of $\omega_1 = 3.50895999$. $t_a/t_c = 0.1$, $\xi_s = 0.5$ and $\xi_e = 0.9$.

Ramos et al. [11] used the position shift technique to "uncouple" the stiffness and mass effects of *E. coli* bacteria by inkjetting them at different positions. We then shift the position of adsorption layer to see if the inverse problem can be solved. In Fig. 4(a), the same myosin layer with $t_a/t_c = 0.1$ is used; the position is shifted towards the clamping end as $\xi_s = 0.5$ and $\xi_e = 0.7$. Now the first resonant frequency becomes as $\omega_1 = 3.513955$, which is the −0.059% smaller than ω_1^0. The same procedure is applied again: ω_1 is computed for various α-β combinations and the level plane is now set with $\omega_1 = 3.513955$. The same intersection line is obtained, which

is to say that the position shifting method can not solve the inverse problem, either. Besides shifting the position of a gold coating layer, Lee et al. [13] also systematically varied the layer length to see how the resonant frequencies change. In Fig. 4(b), we double the layer length by setting $\xi_s = 0.5$ and $\xi_e = 0.9$ to see if the inverse problem is solvable. Now the first resonant frequency becomes as $\omega_1 = 3.50895999$, which is −0.2% smaller than ω_1^0. Again, by setting level plane of $\omega_1 = 3.50895999$, the same intersection line is obtained. In summary, for a given layer with a fixed thickness, the methods of multiple resonant frequencies, shifting the layer position and changing the layer length cannot solve the inverse problem though they can be used to identify the maximum mass and stiffness effects [11,13]. The methods all lead to the same line as presented in Fig. 5. Although these methods narrow down all the possible α-β combinations into a line, it is still an infinite combination. In Fig. 5, the real combination of $(\alpha, \beta) = (1.5070698 \times 10^{-3}, 8.206278 \times 10^{-3})$ is a point (marked as a circle) on the line.

To solve the inverse problem, we vary the layer thickness and utilize its geometry. Two adsorbate layers with different thickness of t_{a1} and t_{a2}, have two corresponding (α_1, β_1) and (α_2, β_2). The following relations are derived from Eq. (6):

$$f_1 = \frac{\alpha_2}{\alpha_1} = \frac{r_2^3 + 3(r_2 + 2r_2^2 + r_2^3)/[1 + (E_a/E_c)r_2]}{r_1^3 + 3(r_1 + 2r_1^2 + r_1^3)/[1 + (E_a/E_c)r_1]}$$

$$\approx \frac{3r_2 + 6r_2^2 + 4r_2^3}{3r_1 + 6r_1^2 + 4r_1^3}, \quad f_2 = \frac{\beta_2}{\beta_1} = \frac{r_2}{r_1} = \frac{t_{a2}}{t_{a1}}, \tag{15}$$

where $r_1 = t_{a1}/t_c$ and $r_2 = t_{a2}/t_c$. The above approximation can be taken because the Young's moduli of many organic and biological materials are very small compared with silicon ($E_c = 169$ GPa). For example, $E_a/E_c = 4/169 \approx 2.367\%$ (alkanethiol), $E_a/E_c = 1.3/169 \approx 0.769\%$ (*E. coli*) and $E_a/E_c = 0.7/169 \approx 0.414\%$ (myosin). The two parameters of f_1 and f_2 only depend on the
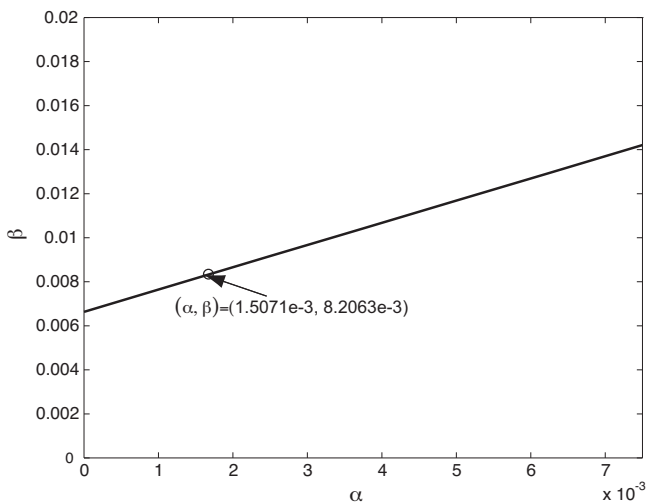
Fig. 5. When the four intersecting lines obtained in Figs. 3 and 4 are projected into the $\alpha - \beta$ plane, the four lines overlap. The real $(\alpha, \beta) = (1.5071 \times 10^{-3}, 8.2053 \times 10^{-3})$ is on the line, which is marked as a circle.

layer thickness (as t_c is fixed). In this method, the thickness of adsorbate layer needs to be measured. However, the thickness measurement is much easier than that of stiffness (Young's modulus) or mass. For example, the adsorbate layer thickness of alkanethiol [21] and DNA [22] was measured by ellipsometry; the thickness of a membrane protein (FhuA) [36] and gold film [13] was measured by atomic force microscope (AFM). It can be even much simpler in a well-controlled inkjetting deposition procedure, in which the volume and spreading shape/area are precisely controlled/monitored [37] and the thickness can thus be easily calculated.

For the myosin layer with $t_{a1} = 0.1\,\mu m$ and $t_{a2} = 0.2\,\mu m$, the exact values of α and β are calculated by Eq. (6) as $(\alpha_1, \beta_1) = (1.5070698 \times 10^{-3}, 8.206278 \times 10^{-3})$ and $(\alpha_2, \beta_2) = (3.6088722 \times 10^{-3}, 1.641256 \times 10^{-2})$. For the full coverage scenario, the following two equations can be obtained by re-arranging Eq. (13)

$$\begin{cases} \sqrt{\dfrac{1+\alpha_1}{1+\beta_1}} - 1 = \dfrac{\omega_1 - \omega_1^0}{\omega_1^0}, \\[3mm] \sqrt{\dfrac{1+\alpha_2}{1+\beta_2}} - 1 = \sqrt{\dfrac{1+f_1\alpha_1}{1+f_2\beta_1}} - 1 = \dfrac{\Omega_1 - \omega_1^0}{\omega_1^0} \end{cases} \quad (16)$$

where $\omega_1 = 3.5043144$ and $\Omega_1 = 3.4937996$ are the first resonant frequencies with (α_1, β_1) and (α_2, β_2), respectively. Once the thickness is measured, $f_1 = 2.416$ and $f_2 = 2$ are calculated by Eq. (15) with $r_1 = t_{a1}/t_c = 0.1$ and $r_2 = t_{a2}/t_c = 0.2$. Because f_1 is obtained by an approximation, it is overestimated by 0.87%. Again, in practice, ω_1^0, ω_1 and Ω_1 are the measured quantities. With the help of Eq. (15), the four unknowns are now reduced to the two (α_1 and β_1). Eq. (16) is solved by the Newton–Rhapson method [34], which gives the computed values of $(\alpha_1^c, \beta_1^c) = (1.5209758 \times 10^{-3}, 8.2163459 \times 10^{-3})$. Compared with the real values of $(\alpha_1, \beta_1) = (1.5070698 \times 10^{-3}, 8.206278 \times 10^{-3})$, the errors are 0.92% and 0.12%, respectively. The computed $(\alpha_2^c, \beta_2^c) = (f_1\alpha_1^c, f_2\beta_1^c) = (3.6436563 \times 10^{-3}, 1.6432692 \times 10^{-3})$. Compared with the real values of $(\alpha_2, \beta_2) = (3.6088722 \times 10^{-3}, 1.641256 \times 10^{-2})$, the errors are 0.96% and 0.12%, respectively.

When $\alpha_1 \ll 1$ and $\beta_1 \ll 1$, the following two approximate linear equations are obtained from Eq. (14)

$$\begin{cases} \dfrac{1}{2}\alpha_1 - \dfrac{1}{2}\beta_1 = \dfrac{\omega_1 - \omega_1^0}{\omega_1^0}, \\[3mm] \dfrac{f_1}{2}\alpha_1 - \dfrac{f_2}{2}\beta_1 = \dfrac{\Omega_1 - \omega_1^0}{\omega_1^0}. \end{cases} \quad (17)$$

The solutions are easily obtained as $\alpha_1 = 2(Q_2 - Q_1 f_2)/(f_1 - f_2)$ and $\beta_1 = 2(Q_2 - Q_1 f_1)/(f_1 - f_2)$, in which $Q_1 = (\omega_1 - \omega_1^0)/\omega_1^0$ and $Q_2 = (\Omega_1 - \omega_1^0)/\omega_1^0$. Compared with the real values of $(\alpha_1, \beta_1) = (1.5070698 \times 10^{-3}, 8.206278 \times 10^{-3})$, the errors of α_1 and β_1 calculated by Eq. (17) are 13.16% and 1.89%, respectively.

In the partial coverage scenario, when ξ_s and ξ_e are given, Eq. (11) actually has the function form of $\mathcal{F}(\omega, \alpha, \beta) = 0$. Here $\xi_s = 0.7$ and $\xi_e = 0.9$ are given. Similar to the full coverage scenario, the following two equations are given for two different thickness cases

$$\begin{cases} \mathcal{F}(\omega_1, \alpha_1, \beta_1) = 0, \\ \mathcal{F}(\Omega_1, \alpha_2, \beta_2) = \mathcal{F}(\Omega_1, f_1\alpha_1, f_2\beta_1) = 0. \end{cases} \quad (18)$$

Here $f_1, f_2, (\alpha_1, \beta_1)$ and (α_2, β_2) are with the same values as those in the full coverage scenario. Because the adsorbate layer length is significantly reduced, the two first resonant frequencies now change to $\omega_1 = 3.5110114$ and $\Omega_1 = 3.5064902$. Again, by substituting these two frequency values into Eq. (18), there are two equations for two unknowns of α_1 and β_1. The two transcendental equations of Eq.

(18) are solved by the Newton–Rhapson method [34]. The computed $(\alpha_1^c, \beta_1^c) = (1.503461 \times 10^{-3}, 8.2026451 \times 10^{-3})$ are with the errors of −0.24% and −0.04%, respectively; the computed $(\alpha_2^c, \beta_2^c) = (f_1\alpha_1^c, f_2\beta_1^c) = (3.6016978 \times 10^{-3}, 1.640529 \times 10^{-2})$ are with the errors of −0.2% and −0.04%, respectively.

For both the full and partial coverage cases, the two first resonant frequencies with two different adsorbate layer thicknesses are used to solve the inverse problem. Because the higher mode has higher sensitivity to detect the frequency shifts [38], the method can be easily applied to the higher mode case by substituting the (measured) resonant frequencies of higher mode into Eq. (16) or (18). The computation is carried out only for a cantilever beam. A clamped-clamped beam has higher resonant frequencies and higher sensitivity [8]. The method can be easily extended to the other type of the beam structure by simply changing the boundary conditions of Eq. (8). Damping is not considered in the model. Small damping is a much sought-after property in the application of micro/nanomechanical resonator. Small damping means high quality factor, which significantly enhances the resonator sensitivity [10,38]. The quality factor of a resonator vibrating in a vacuum can be as high as 10^4 to 10^5 [10]. Therefore, the damping effect is ignored in many modelings of the resonator vibration in air or vacuum [11–13]. A generalized eigenvalue problem formulation of a beam with the damping effect is presented in reference [39].

Although the method of solving the inverse problem requires the measurement of the adsorbate thickness, it actually gives us a way to identify what kind of material the adsorbate is. The above method only detect the mass and stiffness changes due to the adsorbate layer, which are also related with its size. With the knowledge of the layer size/thickness, the mass density and Young's modulus of an adsorbate can be easily determined by Eq. (6), which are the intrinsic material properties. A lot of materials can be identified by these two material properties.

4. Summary

The method for solving the inverse problem, which is to use the shifts of resonant frequency to determine the stiffness and mass, is presented. By varying the adsorbate layer thickness and using a geometric approximation, two independent equations are obtained to solve the two unknowns: stiffness and mass. Because of the small Young's modulus and thickness of biochemical adsorbate, the shifts of the resonant frequencies are very small. To minimize the computation error, an analytical solution is derived for the full coverage scenario and an exact method for the resonant frequency computation is presented for the partial coverage scenario. Although the numerical computation is still required by the exact method, it eliminates the error caused by the mode shape deviation. The computation error of the method are from three sources: (1) the geometric approximation of Eq. (15); (2) the Newton–Rhapson method of solving the nonlinear equations; (3) for Eq. (14), the error is mainly due to the linear approximation. The accuracy of the method is also demonstrated. As the inverse problem is solved for the no damping case, damping should be considered to achieve a higher accuracy in a real application. The method should be of some help to the resonator application by extracting more information from the shifts of resonant frequency.

Appendix A. Definition of K

$$
\mathbf{K} = \begin{pmatrix}
0 & k_{1,2} & 0 & k_{1,4} & 0 & 0 & 0 & 0 & 0 & 0 & 0 & 0 \\
k_{2,1} & 0 & k_{2,3} & 0 & 0 & 0 & 0 & 0 & 0 & 0 & 0 & 0 \\
0 & 0 & 0 & 0 & 0 & 0 & 0 & 0 & k_{3,9} & k_{3,10} & k_{3,11} & k_{3,12} \\
0 & 0 & 0 & 0 & 0 & 0 & 0 & 0 & k_{4,9} & k_{4,10} & k_{4,11} & k_{4,12} \\
k_{5,1} & k_{5,2} & k_{5,3} & k_{5,4} & k_{5,5} & k_{5,6} & k_{5,7} & k_{5,8} & 0 & 0 & 0 & 0 \\
k_{6,1} & k_{6,2} & k_{6,3} & k_{6,4} & k_{6,5} & k_{6,6} & k_{6,7} & k_{6,8} & 0 & 0 & 0 & 0 \\
k_{7,1} & k_{7,2} & k_{7,3} & k_{7,4} & k_{7,5} & k_{7,6} & k_{7,7} & k_{7,8} & 0 & 0 & 0 & 0 \\
k_{8,1} & k_{8,2} & k_{8,3} & k_{8,4} & k_{8,5} & k_{8,6} & k_{8,7} & k_{8,8} & 0 & 0 & 0 & 0 \\
0 & 0 & 0 & 0 & k_{9,5} & k_{9,6} & k_{9,7} & k_{9,8} & k_{9,9} & k_{9,10} & k_{9,11} & k_{9,12} \\
0 & 0 & 0 & 0 & k_{10,5} & k_{10,6} & k_{10,7} & k_{10,8} & k_{10,9} & k_{10,10} & k_{10,11} & k_{10,12} \\
0 & 0 & 0 & 0 & k_{11,5} & k_{11,6} & k_{11,7} & k_{11,8} & k_{11,9} & k_{11,10} & k_{11,11} & k_{11,12} \\
0 & 0 & 0 & 0 & k_{12,5} & k_{12,6} & k_{12,7} & k_{12,8} & k_{12,9} & k_{12,10} & k_{12,11} & k_{12,12}
\end{pmatrix}
$$

$k_{1,2} = 1$, $k_{1,4} = 1$

$k_{2,1} = 1$, $k_{2,3} = 1$

$k_{3,9} = -\sin\kappa_1$, $k_{3,10} = -\cos\kappa_1$, $k_{3,11} = \sinh\kappa_1$, $k_{3,12} = \cosh\kappa_1$

$k_{4,9} = -\cos\kappa_1$, $k_{4,10} = \sin\kappa_1$, $k_{4,11} = \cosh\kappa_1$, $k_{4,12} = \sinh\kappa_1$

$k_{5,1} = \sin(\kappa_1\xi_s)$, $k_{5,2} = \cos(\kappa_1\xi_s)$, $k_{5,3} = \sinh(\kappa_1\xi_s)$, $k_{5,4} = \cosh(\kappa_1\xi_s)$, $k_{5,5} = -\sin(\kappa_2\xi_s)$, $k_{5,6} = -\cos(\kappa_2\xi_s)$, $k_{5,7} = -\sinh(\kappa_2\xi_s)$, $k_{5,8} = -\cosh(\kappa_2\xi_s)$

$k_{6,1} = \cos(\kappa_1\xi_s)$, $k_{6,2} = -\sin(\kappa_1\xi_s)$, $k_{6,3} = \cosh(\kappa_1\xi_s)$, $k_{6,4} = \sinh(\kappa_1\xi_s)$, $k_{6,5} = -\frac{\kappa_2}{\kappa_1}\cos(\kappa_2\xi_s)$, $k_{6,6} = \frac{\kappa_2}{\kappa_1}\sin(\kappa_2\xi_s)$, $k_{6,7} = -\frac{\kappa_2}{\kappa_1}\cosh(\kappa_2\xi_s)$, $k_{6,8} = -\frac{\kappa_2}{\kappa_1}\sin(\kappa_2\xi_s)$

$k_{7,1} = -\sin(\kappa_1\xi_s)$, $k_{7,2} = -\cos(\kappa_1\xi_s)$, $k_{7,3} = \sinh(\kappa_1\xi_s)$, $k_{7,4} = \cosh(\kappa_1\xi_s)$, $k_{7,5} = \frac{\kappa_2^2}{\kappa_1^2}\sin(\kappa_2\xi_s)$, $k_{7,6} = \frac{\kappa_2^2}{\kappa_1^2}\cos(\kappa_2\xi_s)$, $k_{7,7} = -\frac{\kappa_2^2}{\kappa_1^2}\sinh(\kappa_2\xi_s)$, $k_{7,8} = -\frac{\kappa_2^2}{\kappa_1^2}\cosh(\kappa_2\xi_s)$

$k_{8,1} = -\cos(\kappa_1\xi_s)$, $k_{8,2} = \sin(\kappa_1\xi_s)$, $k_{8,3} = \cosh(\kappa_1\xi_s)$, $k_{8,4} = \sinh(\kappa_1\xi_s)$, $k_{8,5} = \frac{\kappa_2^3}{\kappa_1^3}\cos(\kappa_2\xi_s)$, $k_{8,6} = -\frac{\kappa_2^3}{\kappa_1^3}\sin(\kappa_2\xi_s)$, $k_{8,7} = -\frac{\kappa_2^3}{\kappa_1^3}\cosh(\kappa_2\xi_s)$, $k_{8,8} = -\frac{\kappa_2^3}{\kappa_1^3}\sinh(\kappa_2\xi_s)$

$k_{9,5} = \sin(\kappa_2\xi_e)$, $k_{9,6} = \cos(\kappa_2\xi_e)$, $k_{9,7} = \sinh(\kappa_2\xi_e)$, $k_{9,8} = \cosh(\kappa_2\xi_e)$, $k_{9,9} = -\sin(\kappa_1\xi_e)$, $k_{9,10} = -\cos(\kappa_1\xi_e)$, $k_{9,11} = -\sinh(\kappa_1\xi_e)$, $k_{9,12} = -\cosh(\kappa_1\xi_e)$

$k_{10,5} = \cos(\kappa_2\xi_e)$, $k_{10,6} = -\sin(\kappa_2\xi_e)$, $k_{10,7} = \cosh(\kappa_2\xi_e)$, $k_{10,8} = \sinh(\kappa_2\xi_e)$, $k_{10,9} = -\frac{\kappa_1}{\kappa_2}\cos(\kappa_1\xi_e)$, $k_{10,10} = \frac{\kappa_1}{\kappa_2}\sin(\kappa_1\xi_e)$, $k_{10,11} = -\frac{\kappa_1}{\kappa_2}\cosh(\kappa_1\xi_e)$, $k_{10,12} = -\frac{\kappa_1}{\kappa_2}\sinh(\kappa_1\xi_e)$

$k_{11,5} = -\sin(\kappa_2\xi_e)$, $k_{11,6} = -\cos(\kappa_2\xi_e)$, $k_{11,7} = \sinh(\kappa_2\xi_e)$, $k_{11,8} = \cosh(\kappa_2\xi_e)$, $k_{11,9} = \frac{\kappa_1^2}{\kappa_2^2}\sin(\kappa_1\xi_e)$, $k_{11,10} = \frac{\kappa_1^2}{\kappa_2^2}\cos(\kappa_1\xi_e)$, $k_{11,11} = -\frac{\kappa_1^2}{\kappa_2^2}\sinh(\kappa_1\xi_e)$, $k_{11,12} = -\frac{\kappa_1^2}{\kappa_2^2}\cosh(\kappa_1\xi_e)$

$k_{12,5} = -\cos(\kappa_2\xi_e)$, $k_{12,6} = \sin(\kappa_2\xi_e)$, $k_{12,7} = \cosh(\kappa_2\xi_e)$, $k_{12,8} = \sinh(\kappa_2\xi_e)$, $k_{12,9} = \frac{\kappa_1^3}{\kappa_2^3}\cos(\kappa_1\xi_e)$, $k_{12,10} = -\frac{\kappa_1^3}{\kappa_2^3}\sin(\kappa_1\xi_e)$, $k_{12,11} = -\frac{\kappa_1^3}{\kappa_2^3}\cosh(\kappa_1\xi_e)$, $k_{12,12} = -\frac{\kappa_1^3}{\kappa_2^3}\sinh(\kappa_1\xi_e)$

References

[1] T.P. Burg, S.R. Manalis, Suspended microchannel resonators for biomolecular detection, Appl. Phys. Lett. 83 (2003) 2698–2700.

[2] T.P. Burg, M. Godin, S.M. Knudsen, W. Shen, G. Carlson, J.S. Foster, K. Babcock, S.R. Manalis, Weighing of biomolecules, single cells and single nanoparticles in fluid, Nature 446 (2007) 1066–1069.

[3] R.G. Knobel, Weighing single atoms with a nanotube, Nat. Nanotechnol. 3 (2008) 525–526.

[4] W.H. Grover, A.K. Bryaan, M. Diez-Silva, S. Suresh, J.M. Higgins, S.R. Manalis, Measuring single-cell density, Proc. Natl. Acad. Sci. U. S. A. 108 (2011) 10992–10996.

[5] A. Gupta, D. Akin, R. Bashir, Single virus particle mass detection using microresonator with nanoscale thickness, Appl. Phys. Lett. 84 (2004) 1976–1978.

[6] M.S. Hanay, S. Kelber, A.K. Naik, D. Chi, S. Hentz, E.C. Bullard, E. Colinet, L. Duraffourg, M.L. Roukes, Single-protein nanomechanical mass spectrometry in real time, Nat. Nanotechnol. 7 (2012) 602–608.

[7] K. Jensen, K. Kim, A. Zettl, An atomic-resolution nanomechanical mass sensor, Nat. Nanotechnol. 3 (2008) 533–537.

[8] J. Chaste, A. Eichler, J. Moser, G. Ceballos, R. Rurali, A. Bachtold, A nanomechanical mass sensor with yoctogram resolution, Nat. Nanotechnol. 7 (2012) 301–304.

[9] K. Eom, H.S. Park, D.S. Yoon, T. Kwon, Nanomechanical resonators and their applications in biological/chemical detection: nanomechanics principles, Phys. Rep. 503 (2011) 115–163.

[10] H. Craighead, Measuring more than mass, Nat. Nanotechnol. 2 (2007) 18–19.

[11] D. Ramos, J. Tamayo, J. Mertens, M. Calleja, A. Zaballos, Origin of the response of nanomechanical resonators to bacteria adsorption, J. Appl. Phys. 100 (2006) 106105.

[12] J. Tamayo, D. Ramos, J. Mertens, M. Calleja, Effect of the adsorbate stiffness on the resonance of microcantilever sensors, Appl. Phys. Lett. 89 (2006) 224104.

[13] D. Lee, S. Kim, N. Jung, T. Thundat, S. Jeon, Effects of gold patterning on the bending profile and frequency response of a microcantilever, Nanotechnology 106 (2009) 024310.

[14] A. Gupta, P.R. Nair, D. Akin, M.R. Ladisch, S. Broyles, M.A. Alam, R. Bashir, Anomalous resonance in a nanomechanical biosensor, Proc. Natl. Acad. Sci. U. S. A. 103 (2006) 13362–13367.

[15] M. Varshney, P.S. Waggoner, C.P. Tan, K. Aubin, R.A. Montage, H.G. Craighead, Prion protein detection using nanomechanical resonator arrays and secondary mass labeling, Anal. Chem. 80 (2008) 2141–2148.

[16] N.V. Lavrik, M.J. Sepaniak, P.G. Datskos, Cantilever transducers as a platform for chemical and biological sensors, Rev. Sci. Instrum. 75 (2004) 2229–2253.

[17] P. Mohanty, D.A. Harrington, K.L. Ekinci, Y.T. Yang, M.J. Murphy, M.L. Roukes, Intrinsic dissipation in high-frequency micromechanical resonator, Phys. Rev. B 66 (2002) 085416.

[18] L. Meirovitch, Analytical Methods in Vibrations, Macmillan Publishing Co. Inc., New York, 1967.

[19] S. Cherian, T. Thundat, Determination of adsorption-induced variation in the spring constant of a microcantilever, Appl. Phys. Lett. 80 (2002) 2219–2221.

[20] M. Álvarez, J. Tamayo, Optical sequential readout of microcantilever arrays for biological detection, Sens. Actuators B 106 (2005) 687–690.

[21] R. Berger, E. Delamarche, H.P. Lang, Ch. Gerber, J.K. Gimzewski, E. Meyer, H.J. Gütherodt, Surface stress in the self-assembly of alkanethiols on gold, Science 276 (1997) 2021–2024.

[22] J. Fritz, M.K. Baller, H.P. Lang, H. Rothuizen, P. Vettiger, E. Meyer, H.J. Gütherodt, Ch. Gerber, J.K. Gimzewski, Translating biomolecular recognition into nanomechanics, Science 288 (2000) 316–318.

[23] Y. Zhang, L. Zhuo, H. Zhao, Determining the effects of surface elasticity and surface stress by measuring the shifts of resonant frequencies, Proc. R. Soc. Lond. A 469 (2013) 20130449.

[24] Y. Zhang, Determining the adsorption-induced surface stress and mass by measuring the shifts of resonant frequencies, Sens. Actuators A 194 (2013) 169–175.

[25] R.B. Karabalin, L.G. Villanueva, M.H. Matheny, J.E. Sader, M.L. Roukes, Stress-induced variations in the stiffness of micro- and nanocantilever beams, Phys. Rev. Lett. 108 (2012) 236101.

[26] E. Finot, A. Fabre, A. Passian, T. Thundat, Dynamic and static manifestation of molecular absorption in thin films probed by a microcantilever, Phys. Rev. Appl. 1 (2014) 024001.

[27] F.M. Battiston, J.P. Ramseyer, H.P. Lang, M.K. Baller, Ch. Gerber, J.K. Gimzewski, E. Meyer, H.J. Gütherodt, A chemical sensor based on a microfabricated cantilever array with simultaneous resonance-frequency and bending readout, Sens. Actuators B 77 (2001) 122–131.

[28] G.Y. Chen, T. Thundat, E.A. Wachter, R.J. Warmack, Adsorption-induced surface stress and its effects on resonant frequency of microcantilevers, J. Appl. Phys. 77 (1995) 3618–3622.

[29] Z. Hu, T. Thundat, R.J. Warmack, Investigation of adsorption and adsorption-induced surface stresses using microcantilever sensors, J. Appl. Phys. 90 (2001) 427–431.

[30] R.H. Farahi, A. Passian, L. Tetard, T. Thundat, Critical issues in sensor science to aid food and water safety, ACS Nano 6 (2012) 4548–4556.

[31] S. Jeon, N. Jung, T. Thundat, Nanomechanics of a self-assembled monolayer on microcantilever sensors measured by a multiple-point deflection technique, Sens. Actuators B 122 (2007) 365–368.

[32] X. Huang, C.A. Zorman, M. Mehregany, M.L. Roukes, Nanodevice motion at microwave frequencies, Nature 421 (2003) 496.

[33] Y. Zhang, Y.P. Zhao, Flexural contact in MEMS stiction, Int. J. Solids Struct. 49 (2012) 2203–2214.

[34] W.H. Press, S.A. Teukolsky, W.T. Vetterling, B.P. Flannery, Numerical Recipes in Fortran, 2nd ed., Cambridge University Press, Cambridge, 1992.

[35] T.C. Chang, R.R. Craig, Normal modes of uniform beams, J. Eng. Mech. 195 (1969) 1027–1031.

[36] T. Braun, M.K. Ghatkesar, N. Backmann, W. Grange, P. Boulanger, L. Letellier, H.P. Lang, A. Bietsch, Ch. Gerber, M. Hegner, Quantitative time-resolved measurement of membrane protein–ligand interactions using microcantilever array sensors, Nat. Nanotechnol. 4 (2009) 179–185.

[37] A. Bietsch, J. Zhang, M. Hegner, H.P. Lang, Ch. Gerber, Rapid functionalization of cantilever sensors by inkjet printing, Nanotechnology 15 (2004) 873–880.

[38] M.K. Ghatkesar, V. Barwich, T. Braun, J. Ramseyer, Ch. Gerber, M. Hegner, H.P. Lang, U. Drechsler, M. Despont, Higher modes of vibration increase mass sensitivity in nanomechanical microcantilever, Nanotechnology 18 (2007) 445502.

[39] Y. Zhang, K.D. Murphy, Multi-modal analysis on the intermittent contact dynamics of atomic force microscope, J. Sound Vibr. 330 (2011) 5569–5582.

Biography

Yin Zhang, BS, Department of Mechanics, Peking University, Beijing, China, 1997 and PhD, Department of Mechanical Engineering, University of Connecticut, Storrs, Connecticut, USA, 2003. From 2003 to 2004, he worked as an assistant professor in the State Key Laboratory of Nonlinear Mechanics (LNM), Institute of Mechanics, Chinese Academy of Sciences (CAS) and as an associate professor from 2004 to 2012, and since 2012, as a professor. His current research focuses on the MEMS/NEMS structural mechanics, dynamics and the inverse problems in the sensors applications.